Published in final edited form as:
Bone. 2012 May ; 50(5): 1115–1122. doi:10.1016/j.bone.2012.01.025.

Activation of resorption in fatigue-loaded bone involves both apoptosis and active pro-osteoclastogenic signaling by distinct osteocyte populations☆

Oran D. Kennedy[a], **Brad C. Herman**[b], **Damien M. Laudier**[a], **Robert J. Majeska**[a], **Hui B. Sun**[b], and **Mitchell B. Schaffler**[a,*]

[a]Department of Biomedical Engineering, The City College of New York, New York, NY 10031, USA

[b]Department of Orthopaedics, Mount Sinai School of Medicine, New York, NY 10029, USA

Abstract

Osteocyte apoptosis is required to initiate osteoclastic bone resorption following fatigue-induced microdamage in vivo; however, it is unclear whether apoptotic osteocytes also produce the signals that induce osteoclast differentiation. We determined the spatial and temporal patterns of osteocyte apoptosis and expression of pro-osteoclastogenic signaling molecules in vivo. Ulnae from female Sprague–Dawley rats (16–18 weeks old) were cyclically loaded to a single fatigue level, and tissues were analyzed 3 and 7 days later (prior to the first appearance of osteoclasts). Expression of genes associated with osteoclastogenesis (RANKL, OPG, VEGF) and apoptosis (caspase-3) were assessed by qPCR using RNA isolated from 6 mm segments of ulnar mid-diaphysis, with confirmation and spatial localization of gene expression performed by immunohistochemistry. A novel double staining immunohistochemistry method permitted simultaneous localization of apoptotic osteocytes and osteocytes expressing pro-osteoclastogenic signals relative to microdamage sites. Osteocyte staining for caspase-3 and osteoclast regulatory signals exhibited different spatial distributions, with apoptotic (caspase 3-positive) cells highest in the damage region and declining to control levels within several hundred microns of the microdamage focus. Cells expressing RANKL or VEGF peaked between 100 and 300 μm from the damage site, then returned to control levels beyond this distance. Conversely, osteocytes in non-fatigued control bones expressed OPG. However, OPG staining was reduced markedly in osteocytes immediately surrounding microdamage. These results demonstrate that while osteocyte apoptosis triggers the bone remodeling response to microdamage, the neighboring non-apoptotic osteocytes are the major source of pro-osteoclastogenic signals. Moreover, both the apoptotic and osteoclast-signaling osteocyte populations are localized in a spatially and temporally restricted pattern consistent with the targeted nature of this remodeling response.

Keywords

In vivo fatigue; Bone; Osteocytes; Apoptosis; RANKL; OPG

☆Conflict of interest: all authors have no conflict of interest.

*Corresponding author at: Department of Biomedical Engineering, The City College of New York, 160 Convent Avenue, Steinman Hall, T-401, NY, NY, 10031, USA. Fax: +1 212 650 6727.

Introduction

Microscopic regions of bone that sustain fatigue microdamage are removed and replaced by the bone remodeling process, which is carried out by a coupled system of osteoclasts and osteoblasts operating in concert as a Basic Multicelluar Unit (BMU) [1–3]. Fatigue damage-induced remodeling, which has been demonstrated in rodent, canine and human bone, effectively replaces damage foci and restores mechanical integrity to the bone tissue [4]. Localized osteocyte apoptosis at microdamage sites plays a central role in 'targeting' remodeling to micro-injury site; indeed when this step is prevented using a pharmacological inhibitor, remodeling does not occur despite the presence of microdamage in the tissue matrix [4]. However, the molecular events that link osteocyte apoptosis to the activation and regulation of the resorptive response are not well understood.

Throughout the body, removal of apoptotic cells occurs by a process involving specialized phagocytic cells from the monocyte macrophage lineage. In bone, this function appears to be carried out by osteoclasts [4–6]. In general, apoptotic cells and their resulting membrane debris have been shown to present cell surface signals for targeted removal. These signals including new molecules that appear on the surface (e.g., phosphatidylserine) and chemically modified surface molecules that are constitutively expressed (e.g. ICAM-3 and CD31) [5,7–10]. This form of signaling, however, requires cell-to-cell or cell-to-debris contact and thus can act only when phagocytic and apoptotic cells are in direct proximity [11]. Achieving direct contact with phagocytic cells like osteoclasts is problematic for dying osteocytes, which are entombed within the bone matrix. Whether apoptotic debris from osteocytes themselves can move through the osteocyte lacunar–canalicular system has not been established, but this seems unlikely since debris size is too large pass through the very small peri-cellular space available for transport in this system [12].

Osteocytes also have the capacity to stimulate osteoclast differentiation via production of essential cytokine signals. Expression of RANKL has been demonstrated in osteocytes [13], and recent studies indicate that selective genetic ablation of RANKL in osteocytes of mice resulted in dramatically impaired resorption during development and a blunted remodeling response to mechanical unloading [14]. Yet while osteocyte apoptosis is an essential prerequisite to the initiation of bone resorption, it is not clear whether the osteocytes undergoing apoptosis are themselves responsible for producing pro-osteoclastogenic signals like RANKL. Apoptotic cells in general are not considered capable of producing the sustained cytokine or other chemical signals required to activate or attract macrophages and related cells such as osteoclasts. In other cases where focal injury leads to localized apoptosis, such as ischemic heart or brain injury, recruitment of phagocytic cells to initiate tissue remodeling is largely carried out by surviving rather than apoptotic cells [15–17]. In other fatigue studies of bone, Verborgt et al. [18] identified two distinct osteocyte populations near microcracks: apoptotic osteocytes immediately surrounding microcracks and surviving neighbor osteocytes that actively protect themselves against cell death by upregulating production of anti-apoptotic proteins such as Bcl-2. Consequently, it seems reasonable to hypothesize that that these actively surviving osteocytes near sites of microdamage may also be an important source of pro-osteoclastogenic signals that orchestrate osteoclast recruitment and activity. To test this hypothesis, we combined candidate gene expression analyses with a novel double immunohistochemistry (IHC) staining technique which allowed us to identify apoptotic osteocytes and simultaneously identify any nearby cells expressing pro-osteoclastogenic signaling molecules following fatigue loading in vivo.

Materials and methods

Ulnar fatigue loading in vivo was used to introduce controlled amounts of bone microdamage, which has been shown to cause osteocyte apoptosis and activate bone remodeling [4]. Ulnae were fatigue-loaded in end load bending and were harvested at 3 and 7 days post fatigue loading. Intracortical resorption is not present until 10–14 days after fatigue loading in this model, thus the 3 and 7 post loading times sampled the activation (pre-resorptive) phase of the remodeling response in this model. Fatigued (FAT) and non-loaded Control (CON) bones were examined using molecular and in situ approaches to evaluate pro-osteoclastogenic signaling by osteocytes.

In vivo fatigue

Fatigue of rat ulnae in vivo using end load bending in has been described in detail elsewhere [19,20]. Briefly, the right ulnae of female Sprague–Dawley rats (FAT group, n=24, 16–18 weeks old, CRL, Charles River MA) were fatigue loaded to a predetermined damage level using an electromagnetic loading system (Electroforce 3200, Bose Corp., MN, USA) at peak loads of 16–18 N at 2 Hz. This load level produces initial peak strains of 3800±500 μstrain [19]. While this range is relatively high compared to strains induced by habitual loading it corresponds well to peak strains reported for bone during vigorous physical exercise [21–26]. Bone tissue loses structural stiffness during the formation of fatigue microdamage [27–31], thus changes in ulna stiffness were monitored from changes in whole bone compliance using the system LVDT. Loading was automatically stopped at a stiffness loss of 25%. This fatigue level has been shown to induce bone microdamage, which causes osteocyte apoptosis and initiates intracortical resorption at the ulnar mid-diaphysis without causing a stress fracture response (i.e., woven bone formation); furthermore, the rat ulna cortex has no baseline intracortical remodeling activity so all remodeling-related changes seen after loading are attributable to the experimental intervention [4,19,20,32]. Loading was carried out under isofluorane anesthesia. Ulnae from an additional group of age and sex matched animals (n = 10) that received no loading were examined as controls. All animals had unrestricted cage activity and ad libitum access to food and water before and after loading. Animals were euthanized, the ulnae dissected free of surrounding soft tissue, and used for either gene expression analyses or immunohistochemical studies as described below. All procedures were conducted under Institutional Animal Care and Use Committee approval.

Gene expression analyses

mRNA levels were measured from mid-diaphyseal segments 6 mm in length (i.e., the principal damage zone in this model) to examine key pro-osteoclastogenic factors: RANKL, OPG, VEGF, and M-CSF. The periosteum was removed from these diaphyses and the mid-diaphyseal segments were flash frozen in liquid nitrogen. At the mid-diaphyseal level, the rat ulna has a unique anatomy with a marrow cavity which is very small, comparable in size to cortical bone blood vessels (Fig. 1). Thus, there is very little bone marrow present in these samples. From a cell population standpoint these samples, having no periosteum and little marrow, constitute an osteocyte-enriched system. Frozen samples were pulverized using a ball mill (Mikro-Dismembrator, Sartorius, Germany) and total RNA was extracted using the RNeasy mini kit (Qiagen) with DNase treatment. RNA was quantified and checked for quality using a Nanodrop spectrophotometer (Thermo Fisher Scientific, Willmington, DE). Reverse transcription was used to synthesize cDNA by using oligo (dT) primers (Invitrogen). Samples of mRNA (5 ng) were analyzed using real-time PCR using a SYBR green detection system to assess relative gene expression; GAPDH was used as housekeeping gene. PCR primer pairs used are shown in Table 1.

Double-staining immunohistochemistry

Immunohistochemistry (IHC) was used to determine the source and location of apoptotic and pro-osteoclastogenic signals in osteocytes. A novel double IHC procedure was developed to allow simultaneous detection of apoptotic cells and cells expressing candidate pro-osteoclastogenic regulatory factors. Samples were decalcified in formic acid, dehydrated in ethylene glycol monoethyl ether, cleared in methyl salicylate and embedded in paraffin. Sections (4 μm thick) were cut from the ulnar mid-diaphyseal region where microdamage, osteocyte apoptosis and bone remodeling occur in this model [4,19,20].

Each section was stained for activated cleaved Caspase-3 (Cas-3) to identify apoptotic cells, and then also for one of three pro-osteoclastogenic signaling molecules: RANKL, OPG and VEGF (Note: M-CSF staining was not included as gene expression studies revealed no changes after fatigue loading). Glass mounted sections were deparaffinized, re-hydrated, treated for 30 min with a methanol– NaOH solution for antigen retrieval (DeCal, Biogenex, San Ramon, CA), then blocked for a further 30 min (Rodent Block R, Biocare Medical, CA). Sections were then incubated overnight in a humidified chamber at 4 °C with a 1:100 dilution of rabbit antibody to cleaved caspase-3 (#9661, Cell Signaling Technologies, Carpinteria, CA) followed by a 30 minute incubation an Alexa Fluor 594-conjugated 2° antibody (A11080, Invitrogen, CA) at 1:700 dilution. Sections were then blocked again for 30 min and incubated with the second primary antibody against RANKL, OPG or VEGF (SC-7628, SC-8468 and SC-7269, Santa Cruz Biotechnology, Santa Cruz CA) overnight at 4 °C as before. An Alexa Fluor 488-conjugated 2° antibody (A11029, Invitrogen, CA) was used for detection of primary antibodies, after which sections were cover-slipped using an aqueous mounting medium. Rat ulnar growth plates processed in an identical manner were used as positive staining controls [33–36]. Species-appropriate negative controls were also examined in each experiment.

Histomorphometry

Sections were examined and images acquired with a 40× magnification objective under fluorescence microscopy using a Zeiss AxioImager microscope equipped with multichannel fluorescence acquisition system (Axiovision, Carl Zeiss Thornwood, NY). Changes in osteocyte expression of apoptotic and regulatory factors were examined as a function of distance from microdamage foci, following a modification of the method of Verborgt et al. [18,20]. A calibrated sampling grid was superimposed over the digital images of microdamage in double stained sections. The numbers of positively stained osteocytes per area (#/mm^2) were then evaluated as function of distance from microdamage in 300 μm × 200 μm regions on either side of the microdamage (Fig. 1). Measurements were made based on the decay pattern of osteocyte signaling over distance reported previously by Verborgt et al. [18] who found that osteocyte expression of both pro- and anti-apoptotic proteins (BAX and BCL-2, respectively) around microdamage foci were localized to within a few hundred microns from microdamage sites. In the current study, in order to fully follow the decay patterns for osteocyte apoptosis or osteoclast regulatory signals until they returned to baseline levels, it was necessary to collect data following a side-to-side axis relative to a microcrack, essentially parallel to the periosteal surfaces, as the distance from damage to the periosteal or endocortical surface was found in preliminary studies to be less than the decay-to-baseline distances.

Statistical analysis

Gene expression and IHC staining distribution data are expressed as mean ± SEM. Differences in candidate gene expression levels in fatigue loaded versus control levels were tested using Student's *t*-test. The Kruskal–Wallis analysis of variance (ANOVA) was used to assess the expression of each factor in osteocytes between groups over distance from the

damage region in all groups. Post-hoc comparisons with control values were performed using the Mann–Whitney *U* test.

Results

Gene expression

Quantitative PCR analysis demonstrated that mRNA levels for RANKL were increased 13 and 24 fold at 3 and 7 days after fatigue loading respectively compared with controls. OPG expression, which is constitutive in osteocytes, was decreased to 65 and 50% of control levels at 3 and 7 days after fatigue loading respectively. The level of VEGF expression, a key promoter of angiogenesis, was also increased at both time-points although the increase (>10 fold increase) was only significant after 7 days. M-CSF expression was present but low and did not increase at either time-point compared with controls (Fig. 2).

Immunohistochemistry

Using our double staining approach we were able to simultaneously visualize both apoptotic cells and those expressing pro-osteoclastogenic signals on the same tissue sections. Fig. 3 shows representative fluorescence photomicrographs from the microdamage regions of sections staining for caspase-3 (Red) and RANKL, OPG, VEGF (Green) in osteocytes from controls group and 3-Day FAT group. Representative negative controls (no primary antibody) are also shown. The vast majority of osteocytes in the measurement region stained for either one or the other of the target ligands, i.e., either Cas-3 or an osteoclast regulatory factor, while very few cells (2–4%) stained simultaneously for two markers. Thus, dying and signaling osteocytes are effectively discrete populations and dying osteocytes themselves do not contribute to production of osteoclast regulatory signals.

RANKL staining was rarely seen in osteocytes in control, non-fatigued bones. At 3 days, strongly stained Cas-3+ osteocytes were found near damage (approximately 60% of all osteocytes, $p<0.001$ compared with controls, Fig. 4A). Their numbers decreased with increasing distance from the damage until returning to control levels by about 200 μm from the damage site. The inverse pattern was seen for RANKL + osteocytes (<10% of all osteocytes) around microdamage, but their numbers increased significantly with distance, peaking at a distance of approximately 200 μm from the damage site (~55% of all osteocytes $p<0.001$ compared with controls), before again returning to baseline levels. At 7 days the staining pattern over distance for each factor was similar to that at 3 days, except numbers Cas-3+ cells in the damage zone were reduced (Fig. 5A). Microcracks were typically located within several hundred microns of the periosteal surface, and RANKL staining in osteocytes extended close to the bone surface (Fig. 6B).

OPG staining was present in osteocytes throughout control, non-fatigued bones. At 3 days after fatigue loading there was strong Cas-3+ staining in osteocytes near damage (~65% of total cells, $p<0.001$ compared with controls, Fig. 4B). Again, their numbers decreased with increasing distance away until returning to baseline. OPG + cells were dramatically reduced at damage sties (<10% of all osteocytes). Their numbers increased with increasing distance from damage and returned to control levels by approximately 200 μm from the damage site. A similar pattern was evident after 7 days with the number of Cas-3+ cells in the damage region again being reduced (Fig. 5B).

VEGF staining was rarely seen in osteocytes in control, non-fatigued bones. At 3 days the number and distribution of Cas-3+ osteocytes followed the same pattern described above. Few VEGF + osteocytes were found near damage but their numbers increased significantly with distance, before returning towards baseline levels, mirroring the pattern seen for RANKL expression. However, VEGF + staining in osteocytes remained elevated at a much

greater distance from the damage site than was seen for RANKL (Fig. 4C). Once again a similar pattern was evident for both factors after 7 day with the only major difference being reduction in the numbers of Cas-3+ cells near damage (Fig. 5C). As was seen for RANKL, VEGF staining in osteocytes extended close to the bone surface (data not shown).

Discussion

Bone remodeling in response to fatigue-induced microdamage is a spatially constrained process where focal tissue injury leads to localized osteocyte apoptosis followed by targeted resorption of the damaged region and its dying cells [18,19,37]. Osteocyte apoptosis also plays an obligatory role in initiating the remodeling response to damage [4], but it is not known if apoptotic osteocytes themselves produce the signals needed to stimulate osteoclast differentiation. The results of this study show that dying and signaling osteocytes are discrete populations. While dying osteocytes did not produce pro-osteoclastogenic signals, a population of non-apoptotic osteocytes surrounding the apoptotic cells near the microdamage zone upregulated expression of RANKL and VEGF and decreased expression of OPG in a spatially and temporally coherent fashion.

The ability of cells within the osteoblast lineage to stimulate osteoclast formation and/or activity was proposed by Rodan and Martin in 1981 [38], but only recently has it become clear that this capacity was maintained and probably enhanced as osteoblasts mature into osteocytes [14,39]. Strikingly, selective ablation of RANKL expression in the osteocyte population in mice led to reduced resorption and its phenotypic consequences during development, and an impaired ability to respond to mechanical unloading [14]. The fatigue microdamage repair model seems particularly well suited to the examination of pro-osteoclastogenic signaling by osteocytes for two reasons. First, baseline intracortical remodeling is zero in this model [19,40]. This appears to differ from some of the mouse studies [14], which were carried out in younger animals where bone resorption rates are higher and more RANKL expression is observed. Consistent with the absence of resorption, we found osteocyte RANKL expression to be negligible by IHC while OPG was constitutively expressed. Second, unlike development and hindlimb unloading, induction of bone remodeling in response to microdamage is highly localized, and allows the relationship between pro-osteoclastogenic signaling to be assessed with respect to both the inducing stimuli (damage and the requisite osteocyte apoptosis) and response (subsequent remodeling). Our findings that a dramatic induction of an increased RANKL/OPG ratio occurred after damage, was limited to a finite region where resorption consistently occurs in this model, and yet extended far enough to reach the periosteal surface where remodeling initiates, strongly support a direct role for osteocytes – specifically non-apoptotic osteocytes – in RANKL based signaling to osteoclast progenitors.

The distribution of osteocytes showing pro-osteoclastogenic signaling characteristics effectively excluded the apoptotic cells, and corresponded to the distribution of viable osteocytes that surrounded fatigue damage and were shown by Verborgt et al. [18] to actively protect themselves from death by upregulating the anti-apoptotic protein Bcl-2. This similarity includes comparable patterns of decline in Bcl-2 expression and pro-osteoclastogenic cytokine expression with increasing distance from microdamage. Whether the population of signaling osteocytes that we observed overlaps fully or partly with the $Bcl\text{-}2^{+}$ population is as yet unclear, but this question can be investigated in future using the double staining approach used in the present study. Also of interest, the distance spanned by the signaling osteocytes relative to the microdamage site (150–200 μm emanating from the damage site) would be sufficient to permit the osteocytederived pro-osteoclastogenic signal to reach the periosteum and its blood supply containing osteoclast progenitors. Finally, the

proapoptotic signal pattern was sustained for at least 7 days post-injury, adequate time for the differentiation of osteoclasts.

The distributions of RANKL and OPG expression following fatigue indicated a shift in the signaling environment surrounding the microdamage area to one favoring osteoclast formation, indicated by upregulation of RANKL and corresponding downregulation of OPG. RANKL is typically formed as a membrane bound molecule (40–45 kDa) which under the appropriate conditions can be cleaved by metalloproteinases into a smaller soluble form(30 kDa) [41]. Immunohistochemical staining cannot distinguish between membrane bound and soluble RANKL in this model system, the available antibodies that work in rodent tissues bind to epitopes that are common to both forms. However, it seems reasonable to hypothesize that osteocyte signaling involves both the membrane bound and soluble forms. The molecular size order for soluble RANKL would allow it to move readily easily through the osteocyte lacunar-canalicular system [12,41]. That up-regulation of RANKL staining in osteocytes is highest some 150–200 μm from the microdamageosteocyte apoptotic core would place this signaling in direct proximity to the nearest bone surface (periosteal or endocortical) at which osteoclast precursors can be recruited. Likewise, OPG, which was found consistently in osteocytes, is a soluble factor that has a molecular size of approximately 60 kDa and should also readily pass through the osteocyte lacunar-canalicular network.

M-CSF has been widely shown to be a necessary factor, along with RANKL, for osteoclastogenesis [42–44]. Surprisingly, we found no change in M-CSF mRNA expression in fatigue-loaded ulnar diaphyses and confirmed this finding in several independent replications of the experiments and analyses. These data show that osteocytes in fatigued bone do not upregulate production of this key regulatory molecule during the osteoclast activation phase in this model. It is possible that the levels of M-CSF expressed constitutively are adequate for osteoclast differentiation following fatigue loading, or that upregulation does occur in a small subpopulation of cells which cannot be detected by these methods. Furthermore, the unique anatomy of the ulnar mid-diaphysis which, as noted earlier, has effectively no marrow cavity, may also play a role. Since M-CSF is produced by marrow stromal cells [45,46], the lack of detectable change in M-CSF expression may be due to the lack of a significant marrow compartment in the rat ulnar diaphysis.

The current experiment revealed that VEGF staining in osteocytes was spatially similar to RANKL, but temporally different. Osteocyte expression of RANKL was significantly increased at 3 days after fatigue, while VEGF production reached significance only at 7 days. VEGF may potentially play several different roles in this system. Expression for this factor is linked to the stabilization of Bcl-2 via the MAP kinase cascade and could contribute to the increased Bcl-2 expression by osteocytes seen by Verborgt et al. as an anti-apoptotic response to microdamage [18,47,48]. Previous studies have also shown VEGF to be involved in the regulation of osteoclastogenesis, both directly and upstream of RANKL [49,50]. However, the late increase in VEGF compared to RANKL appears most consistent with a role in regulating angiogenesis – also an essential element of bone remodeling – and suggests that osteocytes may play a central role in the coordination of this process as well. Since the current studies were limited to times before the appearance of new remodeling spaces and their neovascular elements in this model, future longer term studies will be needed to directly test this hypothesis.

In summary, our results demonstrate clear spatial and temporal relationships between injury, osteocyte apoptosis and pro-osteoclastogenic signaling in response to fatigue-induced microdamage. This represents the first demonstration, to our knowledge, of pro-osteoclastogenic signaling by osteocytes in the context of a targeted bone remodeling

process. These results provide evidence that RANKL expression by osteocytes is low or absent in adult cortical bone osteocytes but is inducible by injury. The finding that apoptotic cells are essential to the initiation of bone remodeling but do not themselves carry out RANKL-based pro-osteoclastogenic signaling indicates a division of labor among osteocytes in response to damage paralleling that seen in ischemic injury. Such similarities suggest that common pathways and mechanisms probably exist in localized remodeling of many tissue types.

Acknowledgments

The authors would like to thank Daniel Leong for help with gene expression analyses and David Fealey for assistance with IHC's. This work was supported by NIH grants AR41210, AR057139 and AR060445 (MBS) and AR050968 (HBS).

References

1. Burr DB, Martin RB, Schaffler MB, Radin EL. Bone remodeling in response to in vivo fatigue microdamage. J Biomech. 1985; 18:189–200. [PubMed: 3997903]
2. Parfitt AM. Bone age, mineral density, and fatigue damage. Calcif Tissue Int. 1993:S82–S85. [discussion S85-6]. [PubMed: 8275385]
3. Schaffler MB. Role of bone turnover in microdamage. Osteoporos Int. 2003; 14(Suppl. 5):S73–S77. [discussion S77-80]. [PubMed: 14504710]
4. Cardoso L, Herman BC, Verborgt O, Laudier D, Majeska RJ, Schaffler MB. Osteocyte apoptosis controls activation of intracortical resorption in response to bone fatigue. J Bone Miner Res. 2009; 24:597–605. [PubMed: 19049324]
5. Fadok VA, Voelker DR, Campbell PA, Cohen JJ, Bratton DL, Henson PM. Exposure of phosphatidylserine on the surface of apoptotic lymphocytes triggers specific recognition and removal by macrophages. J Immunol. 1992; 148:2207–2216. [PubMed: 1545126]
6. Fadok VA, Bratton DL, Guthrie L, Henson PM. Differential effects of apoptotic versus lysed cells on macrophage production of cytokines: role of proteases. J Immunol. 2001; 166:6847–6854. [PubMed: 11359844]
7. Fadok VA, Bratton DL, Konowal A, Freed PW, Westcott JY, Henson PM. Macrophages that have ingested apoptotic cells in vitro inhibit proinflammatory cytokine production through autocrine/paracrine mechanisms involving TGF-beta, PGE2, and PAF. J Clin Invest. 1998; 101:890–898. [PubMed: 9466984]
8. Fadok VA, Henson PM. Apoptosis: giving phosphatidylserine recognition an assist—with a twist. Curr Biol. 2003; 13:R655–R657. [PubMed: 12932346]
9. Henson PM, Bratton DL, Fadok VA. Apoptotic cell removal. Curr Biol. 2001; 11:R795–R805. [PubMed: 11591341]
10. Henson PM, Bratton DL, Fadok VA. The phosphatidylserine receptor: a crucial molecular switch? Nat Rev Mol Cell Biol. 2001; 2:627–633. [PubMed: 11483996]
11. Kogianni G, Mann V, Ebetino F, Nuttall M, Nijweide P, Simpson H, et al. Fas/CD95 is associated with glucocorticoid-induced osteocyte apoptosis. Life Sci. 2004; 75:2879–2895. [PubMed: 15454340]
12. Wang L, Ciani C, Doty SB, Fritton SP. Delineating bone's interstitial fluid pathway in vivo. Bone. 2004; 34:499–509. [PubMed: 15003797]
13. Mueller RJ, Richards RG. Immunohistological identification of receptor activator of NF-kappaB ligand (RANKL) in human, ovine and bovine bone tissues. J Mater Sci Mater Med. 2004; 15:367–372. [PubMed: 15332601]
14. Xiong J, Onal M, Jilka RL, Weinstein RS, Manolagas SC, O'Brien CA. Matrix-embedded cells control osteoclast formation. Nat Med. 2011 Sep 11; 17(10):1235–1241. [PubMed: 21909103]
15. Bederson JB, Levy AL, Ding WH, Kahn R, DiPerna CA, Jenkins AL III, et al. Acute vasoconstriction after subarachnoid hemorrhage. Neurosurgery. 1998; 42:352–360. [discussion 360-2]. [PubMed: 9482187]

16. Desmouliere A, Badid C, Bochaton-Piallat ML, Gabbiani G. Apoptosis during wound healing, fibrocontractive diseases and vascular wall injury. Int J Biochem Cell Biol. 1997; 29:19–30. [PubMed: 9076938]

17. Fisher M. The ischemic penumbra: identification, evolution and treatment concepts. Cerebrovasc Dis. 2004; 17(Suppl. 1):1–6. [PubMed: 14694275]

18. Verborgt O, Tatton NA, Majeska RJ, Schaffler MB. Spatial distribution of Bax and Bcl-2 in osteocytes after bone fatigue: complementary roles in bone remodeling regulation? J Bone Miner Res. 2002; 17:907–914. [PubMed: 12009022]

19. Bentolila V, Boyce TM, Fyhrie DP, Drumb R, Skerry TM, Schaffler MB. Intracortical remodeling in adult rat long bones after fatigue loading. Bone. 1998; 23:275–281. [PubMed: 9737350]

20. Verborgt O, Gibson GJ, Schaffler MB. Loss of osteocyte integrity in association with microdamage and bone remodeling after fatigue in vivo. J Bone Miner Res. 2000; 15:60–67. [PubMed: 10646115]

21. Nunamaker DM, Butterweck DM, Provost MT. Fatigue fractures in thoroughbred racehorses: relationships with age, peak bone strain, and training. J Orthop Res. 1990; 8:604–611. [PubMed: 2355300]

22. Ekenman I, Milgrom C, Finestone A, Begin M, Olin C, Arndt T, et al. The role of biomechanical shoe orthoses in tibial stress fracture prevention. Am J Sports Med. 2002; 30:866–870. [PubMed: 12435654]

23. Burr DB, Milgrom C, Fyhrie D, Forwood M, Nyska M, Finestone A, et al. In vivo measurement of human tibial strains during vigorous activity. Bone. 1996; 18:405–410. [PubMed: 8739897]

24. Milgrom C, Finestone A, Novack V, Pereg D, Goldich Y, Kreiss Y, et al. The effect of prophylactic treatment with risedronate on stress fracture incidence among infantry recruits. Bone. 2004; 35:418–424. [PubMed: 15268892]

25. Milgrom C, Finestone A, Sharkey N, Hamel A, Mandes V, Burr D, et al. Metatarsal strains are sufficient to cause fatigue fracture during cyclic overloading. Foot Ankle Int. 2002; 23:230–235. [PubMed: 11934065]

26. Milgrom C, Radeva-Petrova DR, Finestone A, Nyska M, Mendelson S, Benjuya N, et al. The effect of muscle fatigue on in vivo tibial strains. J Biomech. 2007; 40:845–850. [PubMed: 16682046]

27. Carter DR, Hayes WC. Compact bone fatigue damage II: a microscopic examination. Clin Orthop. 1977; 1977:265–274. [PubMed: 912990]

28. Caler WE, Carter DR, Harris WH. Techniques for implementing an in vivo bone strain gage system. J Biomech. 1981; 14:503–507. [PubMed: 7276010]

29. Schaffler MB, Burr DB. Stiffness of compact bone: effects of porosity and density. J Biomech. 1988; 21:13–16. [PubMed: 3339022]

30. Vashishth D. Rising crack-growth-resistance behavior in cortical bone: implications for toughness measurements. J Biomech. 2004; 37:943–946. [PubMed: 15111083]

31. Vashishth D, Koontz J, Qiu SJ, Lundin-Cannon D, Yeni YN, Schaffler MB, et al. In vivo diffuse damage in human vertebral trabecular bone. Bone. 2000; 26:147–152. [PubMed: 10678409]

32. Silva MJ, Touhey DC. Bone formation after damaging in vivo fatigue loading results in recovery of whole-bone monotonic strength and increased fatigue life. J Orthop Res. 2007; 25:252–261. [PubMed: 17106875]

33. Ballock RT, O'Keefe RJ. The biology of the growth plate. J Bone Joint Surg Am. 2003; 85-A:715–726. [PubMed: 12672851]

34. Ohashi N, Robling AG, Burr DB, Turner CH. The effects of dynamic axial loading on the rat growth plate. J Bone Miner Res. 2002; 17:284–292. [PubMed: 11811559]

35. Silvestrini G, Ballanti P, Patacchioli F, Leopizzi M, Gualtieri N, Monnazzi P, et al. Detection of osteoprotegerin (OPG) and its ligand (RANKL) mRNA and protein in femur and tibia of the rat. J Mol Histol. 2005; 36:59–67. [PubMed: 15704000]

36. Schipani E, Ryan HE, Didrickson S, Kobayashi T, Knight M, Johnson RS. Hypoxia in cartilage: HIF-1alpha is essential for chondrocyte growth arrest and survival. Genes Dev. 2001; 15:2865–2876. [PubMed: 11691837]

37. Frost HM. Presence of microscopic cracks in vivo in bone. Henry Ford Hosp Med Bull. 1960; 8:27–35.
38. Rodan GA, Martin TJ. Role of osteoblasts in hormonal control of bone resorption—a hypothesis. Calcif Tissue Int. 1981; 33:349–351. [PubMed: 6271355]
39. Nakashima T, Hayashi M, Fukunaga T, Kurata K, Oh-Hora M, Feng JQ, et al. Evidence for osteocyte regulation of bone homeostasis through RANKL expression. Nat Med. 2011 Sep 11; 17(10):1231–1234. [PubMed: 21909105]
40. Baron R, Tross R, Vignery A. Evidence of sequential remodeling in rat trabecular bone — morphology, dynamic histomorphometry, and changes during skeletal maturation. Anat Rec. 1984; 208:137–145. [PubMed: 6711834]
41. Nakashima T, Kobayashi Y, Yamasaki S, Kawakami A, Eguchi K, Sasaki H, et al. Protein expression and functional difference of membrane-bound and soluble receptor activator of NF-kappaB ligand: modulation of the expression by osteotropic factors and cytokines. Biochem Biophys Res Commun. 2000; 275:768–775. [PubMed: 10973797]
42. Soderstrom K, Stein E, Colmenero P, Purath U, Muller-Ladner U, de Matos CT, et al. Natural killer cells trigger osteoclastogenesis and bone destruction in arthritis. Proc Natl Acad Sci USA. 2010; 107:13028–13033. [PubMed: 20615964]
43. Feng X, Takeshita S, Namba N, Wei S, Teitelbaum SL, Ross FP. Tyrosines 559 and 807 in the cytoplasmic tail of the macrophage colony-stimulating factor receptor play distinct roles in osteoclast differentiation and function. Endocrinology. 2002; 143:4868–4874. [PubMed: 12446614]
44. Boyle WJ, Simonet WS, Lacey DL. Osteoclast differentiation and activation. Nature. 2003; 423:337–342. [PubMed: 12748652]
45. Udagawa N, Takahashi N, Akatsu T, Tanaka H, Sasaki T, Nishihara T, et al. Origin of osteoclasts: mature monocytes and macrophages are capable of differentiating into osteoclasts under a suitable microenvironment prepared by bone marrow-derived stromal cells. Proc Natl Acad Sci USA. 1990; 87:7260–7264. [PubMed: 2169622]
46. Ross FP. M-CSF, c-Fms, and signaling in osteoclasts and their precursors. Ann N Y Acad Sci. 2006; 1068:110–116. [PubMed: 16831911]
47. Dias S, Shmelkov SV, Lam G, Rafii S. VEGF(165) promotes survival of leukemic cells by Hsp90-mediated induction of Bcl-2 expression and apoptosis inhibition. Blood. 2002; 99:2532–2540. [PubMed: 11895790]
48. Al-Dujaili SA, Lau E, Al-Dujaili H, Tsang K, Guenther A, You L. Apoptotic osteocytes regulate osteoclast precursor recruitment and differentiation in vitro. J Cell Biochem. 2011 Sep 11; 112(9): 2412–2423. [PubMed: 21538477]
49. Sipola A, Nelo K, Hautala T, Ilvesaro J, Tuukkanen J. Endostatin inhibits VEGF-A induced osteoclastic bone resorption in vitro. BMC Musculoskelet Disord. 2006; 7:56. [PubMed: 16839420]
50. Yang Q, McHugh KP, Patntirapong S, Gu X, Wunderlich L, Hauschka PV. VEGF enhancement of osteoclast survival and bone resorption involves VEGF receptor-2 signaling and beta3-integrin. Matrix Biol. 2008; 27:589–599. [PubMed: 18640270]

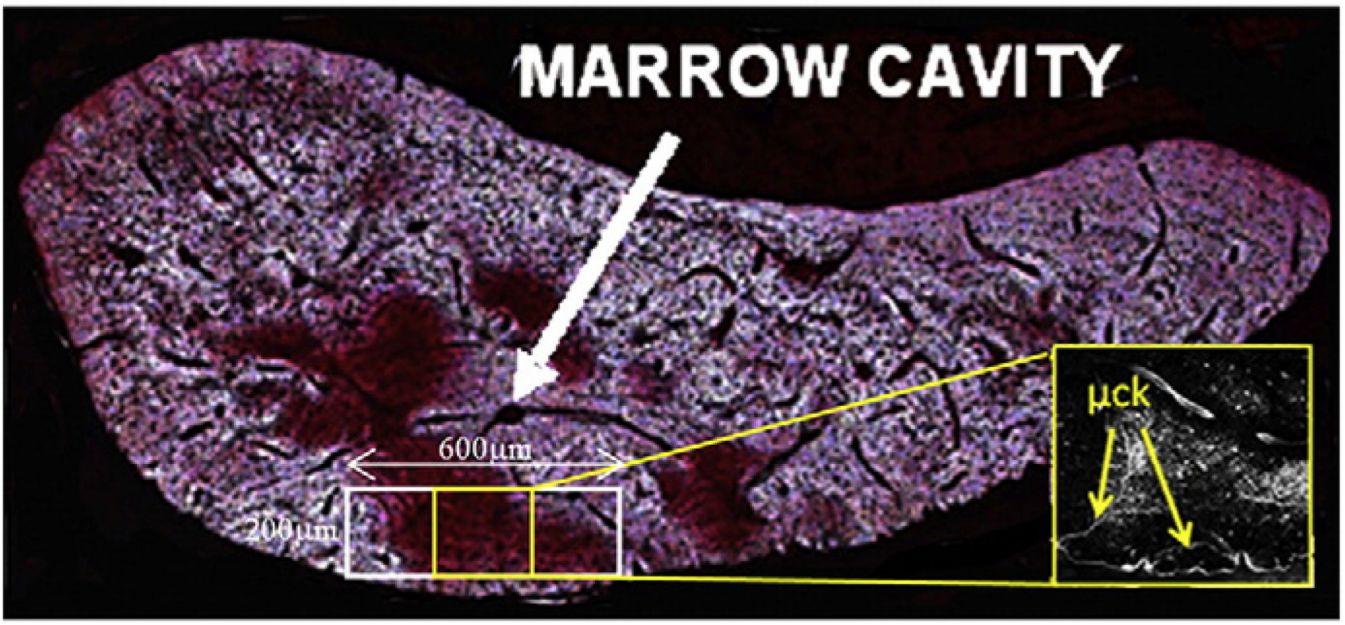

Fig. 1.

Undecalcified cross section of fatigued rat ulnar diaphysis (thickness: 100 μm) showing negligible marrow cavity (white arrow) and basic fuchsin stained damage region in the cortex. Also shown is the measurement scheme for osteocyte apoptosis and factor expression. Inset: Confocal photomicrograph of basic fuchsin stained section showing linear microcracks in center of sampling region.

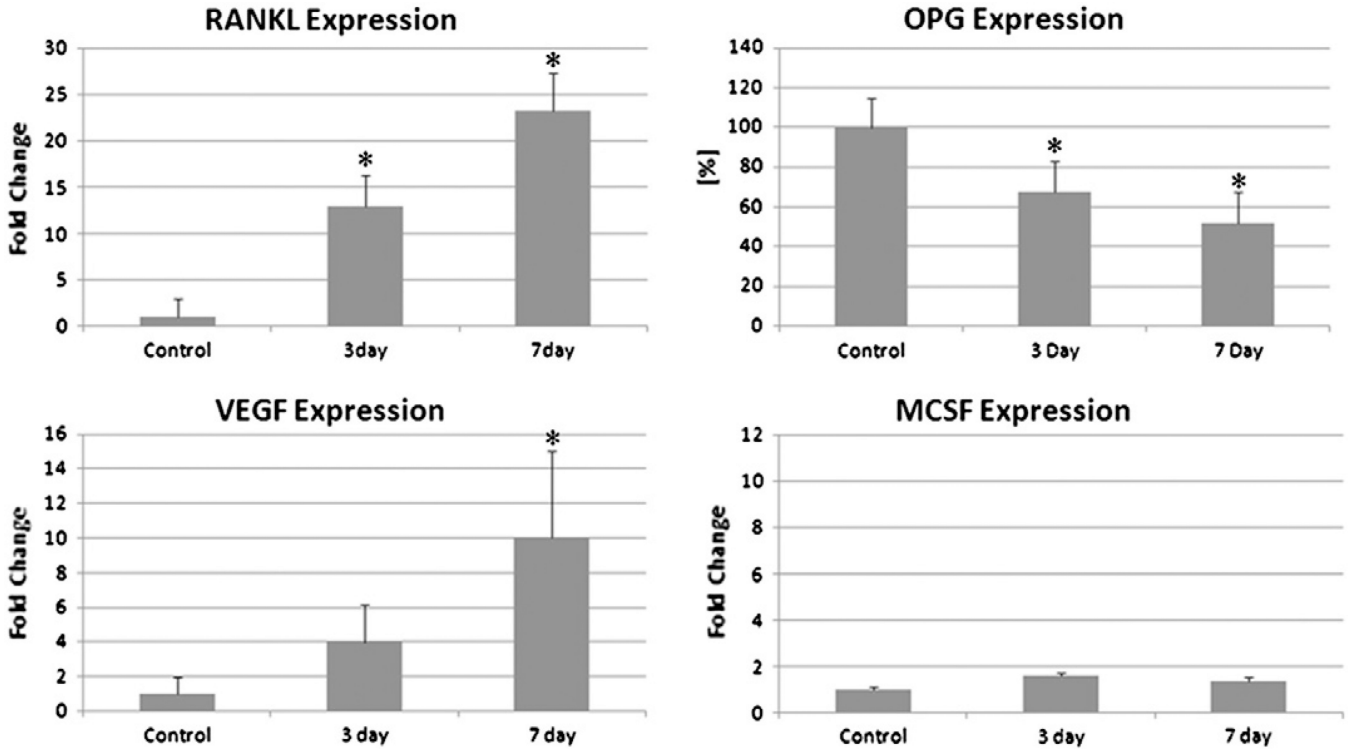

Fig. 2.

Gene expression of osteoclastogenic factors: RANKL, OPG, VEGF and M-CSF from osteocyte enriched segment of rat ulnar cortex at 3 and 7 days after fatigue loading (* = $p<0.001$).

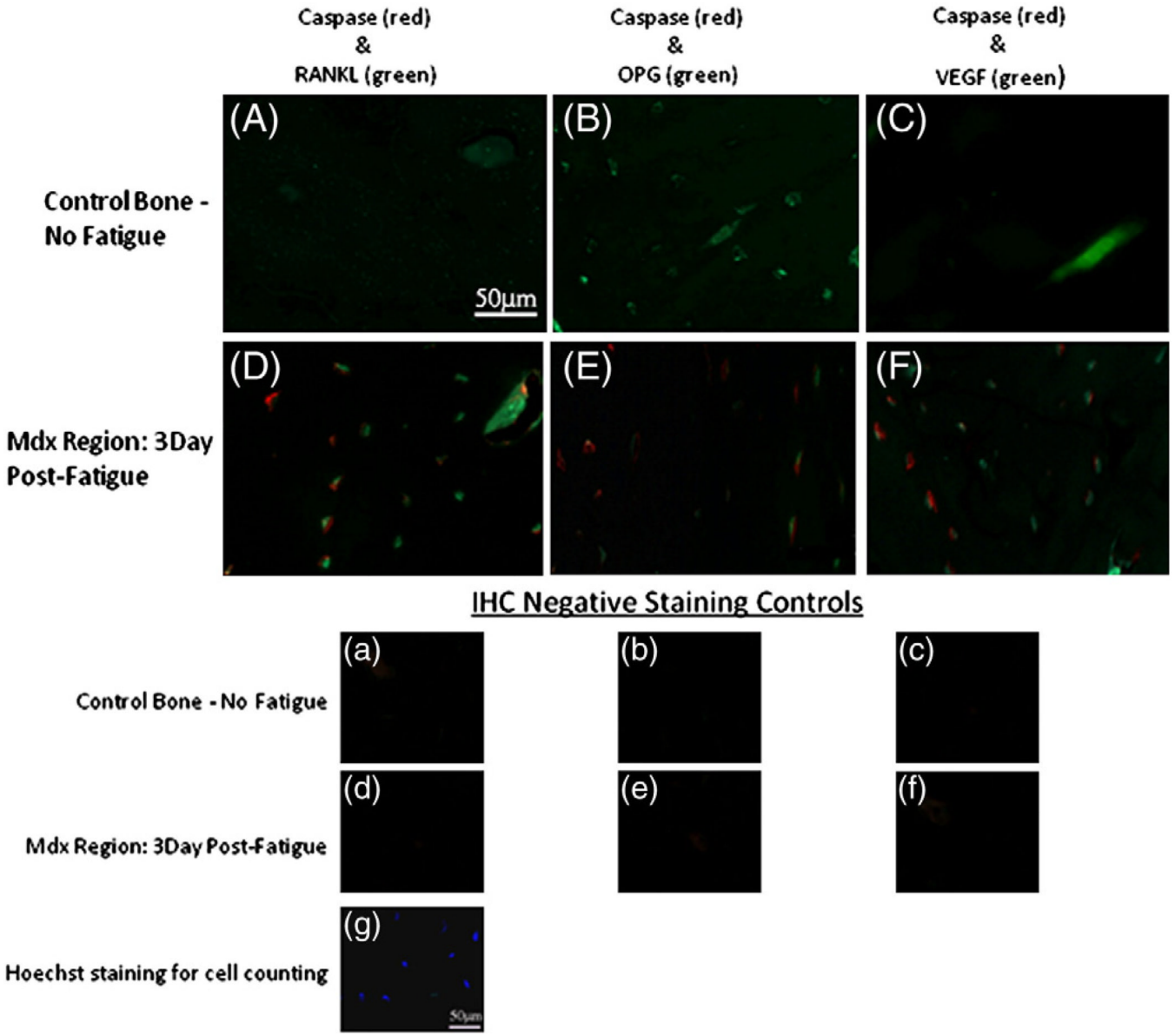

Fig. 3.

Fluorescence photomicrographs of IHC double-staining from the microdamage (Mdx Region, microcrack located at lower left corner in all images) of fatigued ulna and same anatomical region of non-loaded control ulna, showing double-staining in osteocytes for Cas-3 (Alexa Fluor 594 — Red) versus RANKL, OPG, VEGF (Alexa Fluor 488 — Green). All images in the fatigued group are from the 3Day survival timepoint. The corresponding negative staining controls (no primary antibodies) for each pair are shown in the lower group of images (a–f), along with a representative image of Hoechst stained section for cell counting. Note that apoptotic (caspase positive) osteocytes are concentrated near to microdamage, while complementary pattern for RANKL, OPG and VEGF change with distance from damage foci. The majority of osteocytes in the measurement region stained for either one or the other of the target ligands very few cells stained simultaneously for two markers. Morphometric data describing differential staining patterns for dying versus

actively signaling osteocytes are shown in Figs. 4 and 5. (For interpretation of the references to color in this figure legend, the reader is referred to the web version of this article.)

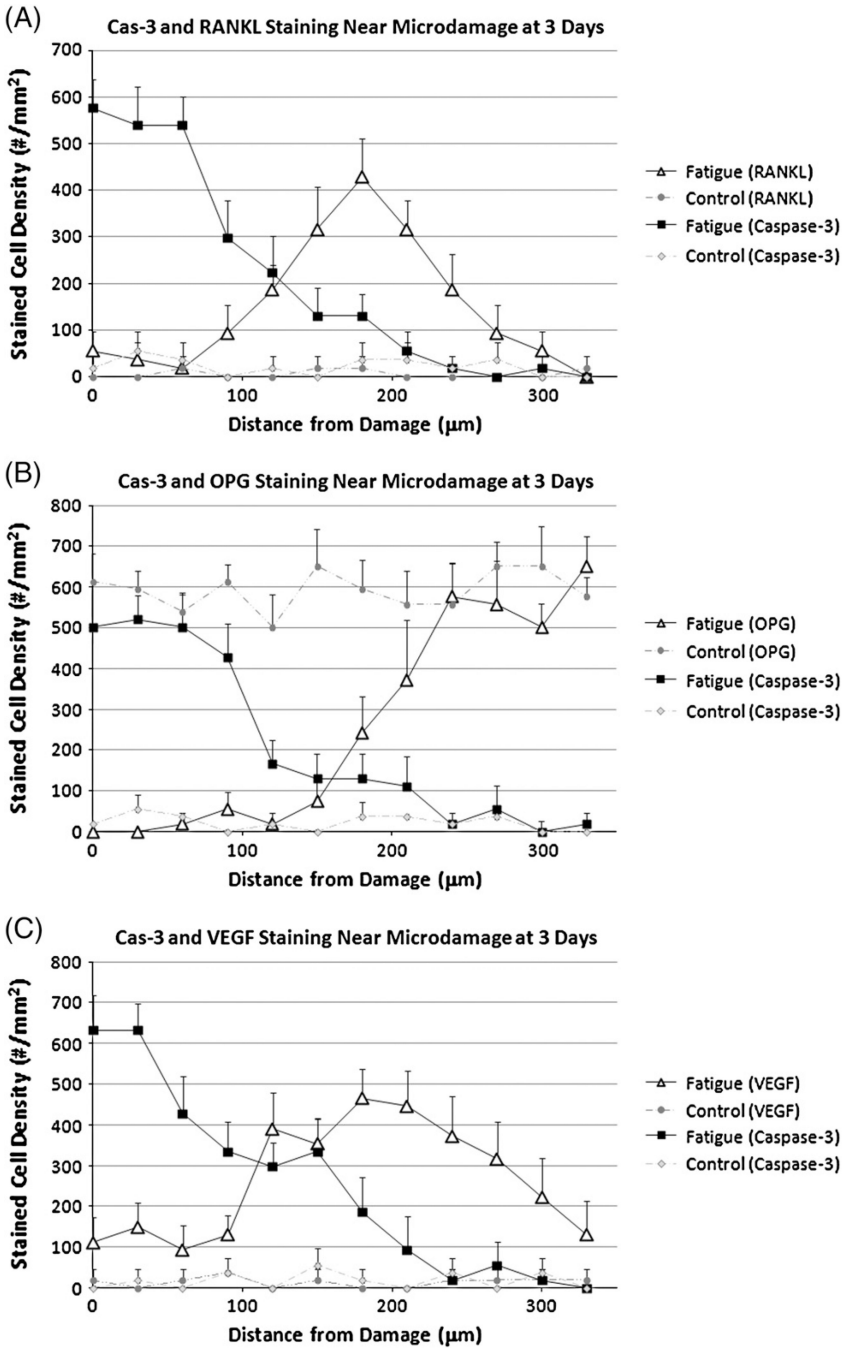

Fig. 4.

Distance distribution showing expression of (A) Cas-3 and RANKL (B) Cas-3 and OPG (C) Cas-3 and VEGF in osteocytes as a function of distance from the damage region 3 days after fatigue loading. (* = $p<0.01$).

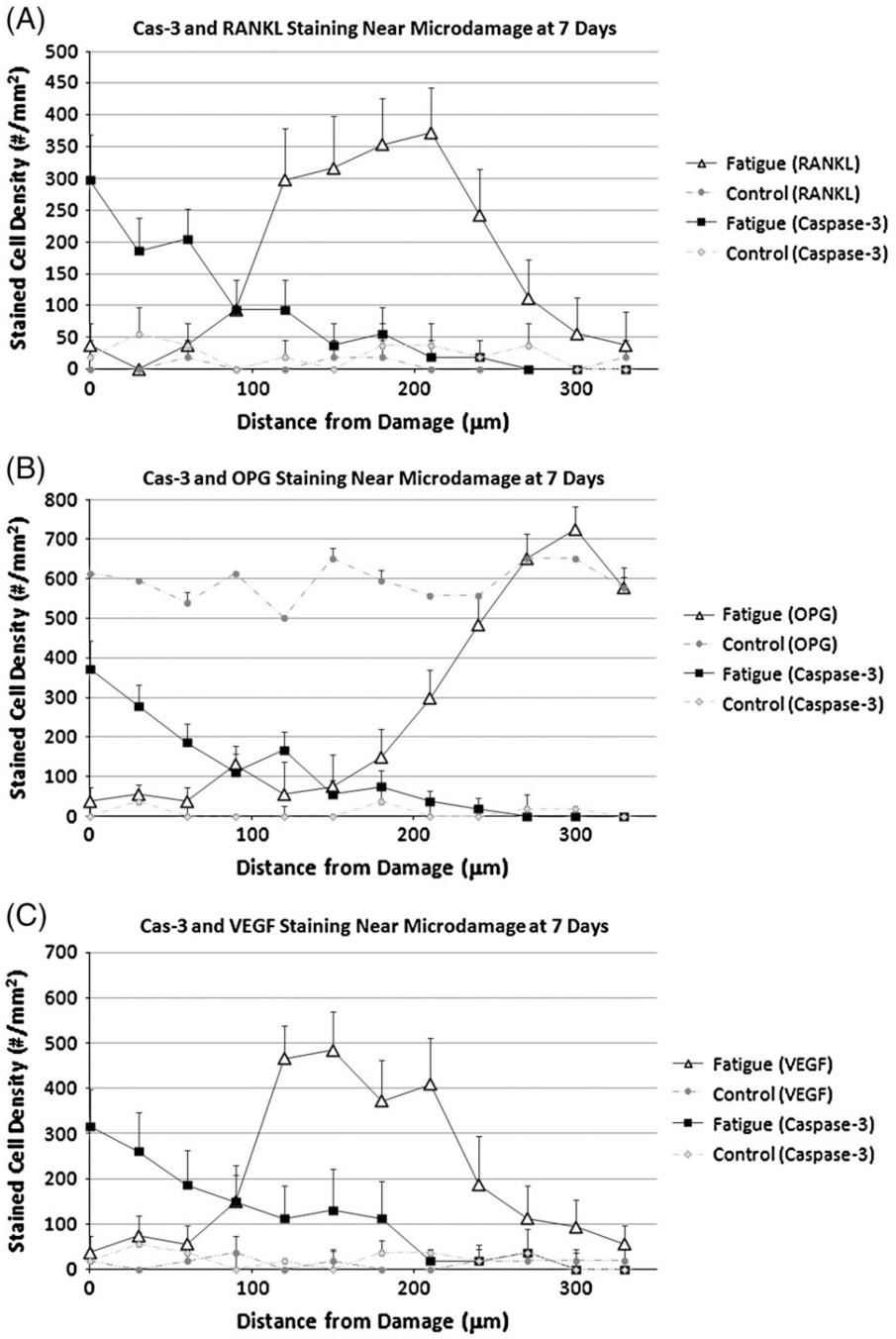

Fig. 5.

Distance distribution showing expression of (A) Cas-3 and RANKL (B) Cas-3 and OPG (C) Cas-3 and VEGF in osteocytes as a function of distance from the damage region 7 days after fatigue loading. (* = $p<0.01$).

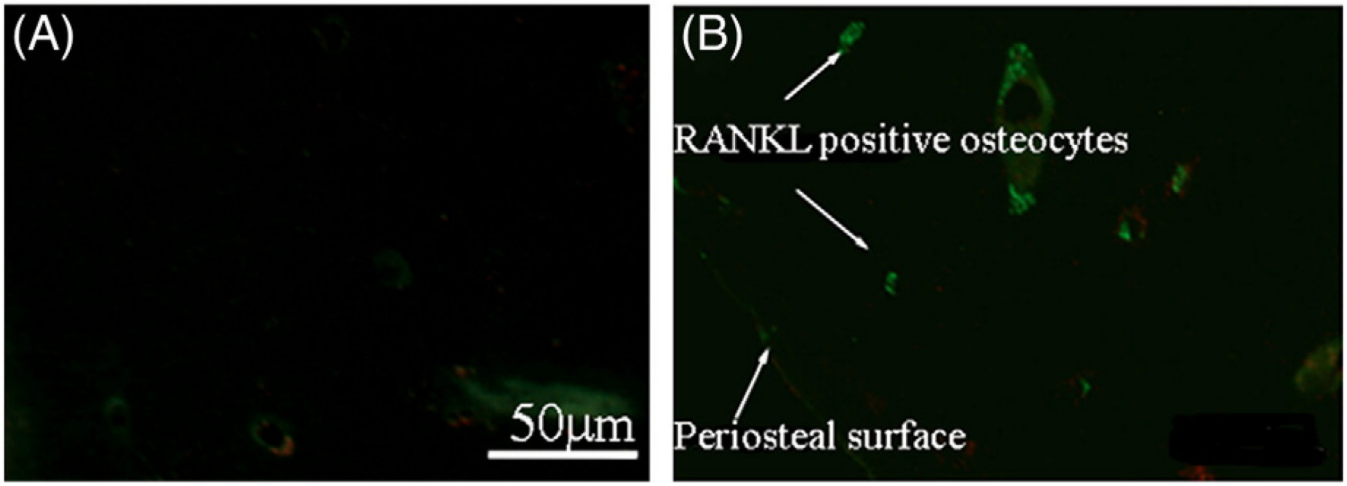

Fig. 6.

Fluorescence photomicrographs of IHC double-stained sections staining for Cas-3 (Red) and RANKL, (Green) in osteocytes from (A) control group and (B) 3-Day FAT group demonstrating that RANKL + osteocytes extend from the microdamage site within the cortex (not visible in this image) to the periosteal bone surface. (For interpretation of the references to color in this figure legend, the reader is referred to the web version of this article.)

Table 1

Candidate gene names and associated PCR primer pair sequences.

	Forward Sequence (5′–3′)	Reverse Sequence (5′–3′)
GAPDH	GAGGACCAGGTTGTCTCCTG	GATGTAGGCCATGAGGGCCAC
RANKL	TGCAGGAGAATGAAACAAGC	ACTGACTTTATGGGAACCCG
OPG	ACACACCAACTGCAGCTCAC	TGTCCACCAGAACACTCAGC
VEGF	CGTCGGAGAGCAACGTCAC	AAACCGGGATTTCTTGCGCT
M-CSF	GGATTCTTCTGTGGGGCGAC	AGGAGCTGTGGTAGTGGCAG